

# Crystallization controlled by layered silicates in nylon 6–clay nano-composite

Yoshihiro Katoh, Masami Okamoto\*

Advanced Polymeric Nanostructured Materials Engineering, Graduate School of Engineering, Toyota Technological Institute, 2-12-1 Hisakata, Tempaku, Nagoya 468 8511, Japan

## ARTICLE INFO

### Article history:

Received 18 March 2009

Accepted 10 July 2009

Available online 16 July 2009

### Keywords:

Nano-composites

Crystallization

Chain mobility

## ABSTRACT

To understand the effect of the montmorillonite (MMT) particles on the crystallization kinetics and crystalline morphology of nylon 6 upon nano-composite formation, we have characterized the crystallization behaviors by using light scattering, wide-angle X-ray diffraction (WAXD), transmission electron microscope (TEM) and rheological measurement. The correlation between the nucleating effect and the growth mechanism of the different polymorphism ( $\gamma$ -phase) of nylon 6 in the nano-composite (N6C3.7) was probed. N6C3.7 exhibited  $\gamma$ -phase crystal due to the nucleating effect of the dispersed MMT particles into the nylon 6 matrix throughout the whole  $T_c$  range (=150–215 °C). The lamellar growth of the  $\gamma$ -phase crystal took place on both sides of the dispersed MMT particles. In comparison between the temperature dependence of the characteristic relaxation time and the crystallization time, the lamellar growth of the  $\gamma$ -phase crystal has been discussed. The stable growth of the  $\gamma$ -phase was strongly disturbed at low  $T_c$  range (=160–190 °C) due to the lack of time for crystallization.

© 2009 Elsevier Ltd. All rights reserved.

## 1. Introduction

Over the last few years, the utility of inorganic nanoscale particles as filler to enhance the polymer performance has been established. Of particular interest is recently developed nano-composite technology consisting of a polymer and organically modified layered filler (organo-clay) because they often exhibit remarkably improved mechanical and various other materials properties as compared with those of virgin polymer or conventional composite (micro/macro-composites) [1–5]. These concurrent property improvements are well beyond what can be generally achieved through the micro/macro-composites preparation.

Toyota group first explored the synthetic strategy and molecular design in nylon 6-based nano-composites (N6NCs) [6–8]. The dispersed montmorillonite (MMT) particles in the N6NCs have some contribution to enhance the nucleation (i.e. nucleating agents) [9,10]. Nylon 6 was crystallized extensively in the  $\gamma$ -form in the nano-composite because of the epitaxial crystallization, which was also revealed from the transmission electron microscopic images [10]. In the pseudo-hexagonal  $\gamma$ -form crystals, the molecular chains have to twist away from the zigzag planes to form hydrogen bonds among the parallel chains in the crystals giving rise to lesser inter-chain interactions compared with the

monoclinic  $\alpha$ -form, which are all-trans and packed in more stable antiparallel-chain arrangement of hydrogen bonds [11].

Mathias et al. [12] have investigated N6NC using  $^{15}\text{N}$  nuclear magnetic resonance and concluded that the MMT particles stabilize the  $\gamma$ -phase of nylon 6. Thus, the formation of the  $\gamma$ -form in the presence of MMT particles is well known [9,10,12–18] and some of the property enhancements of N6NCs [6–8] are reported in the literature.

Besides the nucleating effect, the MMT surfaces (silicate layers) can also clearly retard the crystal growth process [14,19]. The MMT-induced reduction of the overall crystallization rate is due to the disruption of lamella growth by the well dispersed MMT particles [14]. Homminga et al. [20] suggested that the silicate layers hinder the diffusion of polymer chains to the crystal growth front and impurity migration away from the growth front takes place. Miltner et al. [21] reported that the interaction between nylon 6 and MMT reduce the mobility of the polymer chain which benefits to form the  $\gamma$ -phase, depending on the nature of the organo-clay (MMT-intercalant). Furthermore, once a percolated network of the dispersed MMT particles is formed, the networks retard crystalline capability as reported by Wang et al. [22].

Despite extensive studies of the polymer crystallization in N6NC systems, the correlation between the nucleating effect and the growth mechanism of the different polymorphism ( $\gamma$ -phase) underlying these observation is not very well explored in the literature.

In this regard, to prove the effect of the dispersed MMT particles on the crystallization kinetics and crystalline morphology of nylon

\* Corresponding author. Tel.: +81 052 809 1861; fax: +81 052 809 1864.  
E-mail address: [okamoto@toyota-ti.ac.jp](mailto:okamoto@toyota-ti.ac.jp) (M. Okamoto).

6 upon nano-composite formation, we have characterized in this work by using light scattering, wide-angle X-ray diffraction (WAXD), transmission electron microscope (TEM) and rheological measurement.

## 2. Experimental section

### 2.1. Materials

The N6NC were kindly supplied by Dr. A. Usuki of Toyota Central R&D Labs. Inc. It was synthesized by *in-situ* polymerization of  $\epsilon$ -caprolactam in lauryl ammonium intercalated montmorillonite in the presence of small amount of 6-aminocaproic acid (the number-average molecular weight  $M_n$  of  $19.7 \times 10^3$  g/mol) for N6C3.7 [10]. The amount of inorganic montmorillonite (MMT) part, obtained from the burning out of organic part, was 3.7% and is designated as N6C3.7. The  $M_n$  of pure nylon 6 polymerized in bulk is  $21.7 \times 10^3$  g/mol.

### 2.2. Crystallization

The dried N6C3.7 pellets were converted into sheets with a thickness of 0.8–1.1 mm by pressing with  $\approx 1$  MPa at 250 °C for 2 min using a hot press. The molded sheets were again annealed at 250 °C for 2 min, and then they were quickly transferred into a hot stage set at the desired crystallization temperature ( $T_c$ ) (=150–215 °C) and crystallized until full solidification (confirmed from the kinetics of crystallization using a polarizing optical microscope (POM)). The crystallized specimens were characterized by using differential scanning calorimeter (DSC), wide-angle X-ray diffraction (WAXD) and transmission electron microscope (TEM).

### 2.3. Differential scanning calorimetry (DSC)

The crystallized specimens were characterized by using temperature-modulated DSC (TMDSC) (TA 2920; TA Instruments) at the heating/cooling rate of 5 °C/min with a heating/cooling cycle of the modulation period of 60 s and an amplitude of  $\pm 0.769$  °C, to determine the crystallization temperature with cooling from melt ( $T_{cc}$ ), the melting temperature ( $T_m$ ) and heat of fusion ( $\Delta H$ ), the DSC was calibrated with Indium before experiments. For the measurement of degree of crystallinity ( $\chi_c$ ) prior to TMDSC analysis, the extra heat absorbed by the crystallites formed during heating had to be subtracted from the total endothermic heat flow due to the melting of the whole crystallites. This can be done according to the principles and procedures described in our previous paper [23]. By considering the melting enthalpy of 100% crystalline nylon 6 ( $\alpha$ -phase as 241 J/g and  $\gamma$ -phase as 239 J/g, respectively [24]), we have estimated the value of the  $\chi_c$  of neat nylon 6 and N6C3.7, and these values are also presented in Table 1.

### 2.4. Wide-angle X-ray diffraction (WAXD)

WAXD analyses were performed for neat nylon 6 and nano-composite using an Mxlabo X-ray diffractometer (MAC Science Co.; 3 kW, graphite monochromator,  $\text{CuK}\alpha$  radiation ( $\lambda_x = 0.154$  nm), operated at 40 kV and 20 mA). Samples were scanned in fixed time

mode with counting time of 2 s at room temperature under diffraction angle ( $2\theta$ ) in the range of 1°–55°.

### 2.5. Transmission electron microscopy (TEM)

Nanoscale structure of N6C3.7 was investigated by means of TEM (H-7100, Hitachi Co.), operating at an accelerating voltage of 100 kV. The ultra thin sections (the edge of the sample sheet perpendicular to the compression mold) with a thickness of 80 nm were microtomed at  $-80$  °C using a Reichert Ultra cut cryo-ultramicrotome after suitably staining the sample with 12 Tungstophosphoric acid at 80 °C for 2 h.

### 2.6. Rayleigh scattering photometry and polarized optical microscope

We have employed time-resolved light scattering (LS) photometry to estimate the overall crystallization rate and its kinetics in the supercooled state of neat nylon 6 and N6C3.7. The thin sample of about 40  $\mu\text{m}$  thickness was quickly transferred from the melt state ( $\sim 250$  °C for 2 min in order to remove the thermal history) to the Linkam hot stage (Linkam RTVMS, Linkam Scientific Instruments, Ltd.), placed in the LS apparatus, set at the predetermined temperature, and immediately after attaining the  $T_c$ , a time-resolved LS measurement was carried out in the temperature range of 150–215 °C in the supercooled state under the quiescent state. It should be mentioned here that there was some time lag between putting the sample on hot stage and to switch on the computer to collect the data which is  $\sim 1$  s, sufficient for the equilibration of temperature. The one-dimensional photometer was equipped with a 38-channel photodiode (PDA: Hamamatsu Photonics Co.) array, which facilitated the angular dependence of scattering angle ( $\theta_{LS}$ ) was covered between 1.4° and 30°. The radiation of polarized He–Ne laser of 632.8 nm wavelengths was used vertically to the sample, and the scattering profile was observed at an azimuthal angle of 45° under  $H_V$  (cross-polarized) alignment. We also used a conventional Polaroid camera (camera length = 100–400 mm, which gave a scattering vector range of  $0.37$ – $4.15 \mu\text{m}^{-1}$ ) to recover the scattering patterns on a photographic film (Fuji FP-100B; ISO = 100) with an exposure time of 1/250 s [25]. The photographs were taken after full solidification of the sample.

We also measured the spherulite growth of neat nylon 6 and N6C3.7 in the temperature range of 150–215 °C. The thin samples were crystallized on the Linkam hot stage mounted on a polarized optical microscope (POM) (Nikon OPTI-PHOTO2-POL), and the developed spherulite was measured with time using a video recording system (Linkam RTVMS, Linkam Scientific Instruments, Ltd.). After complete crystallization, the samples were observed using POM and fitted with a color-sensitive plate to determine the sign of birefringence, and then photographs were taken. The details regarding POM observation can be found in our previous paper [25].

### 2.7. Melt rheology

Melt rheological measurements were conducted on a RDAII instrument with a torque transducer capable of measurements in the range of 0.2–200 g cm. Dynamic oscillatory shear measurements were performed by applying a time dependent strain of  $\gamma(t) = \gamma_0 \sin(\omega t)$  and the resultant shear stress is  $\sigma(t) = \gamma_0 [G' \sin(\omega t) + G'' \cos(\omega t)]$ , with  $G'$  and  $G''$  being the storage and loss modulus, respectively. Measurements were conducted by using a set of 25 mm diameter parallel plates with a sample thickness of  $\sim 0.8$  mm and in the temperature range of 225–255 °C. The strain

**Table 1**  
TMDSC properties of neat nylon6 and its nano-composite.

Samples	$T_{cc}/^\circ\text{C}$	$T_m/^\circ\text{C}$	$\Delta H_{rev}/\text{J/g}$	$\Delta H_{nonrev}/\text{J/g}$	$\Delta H_{diff}/\text{J/g}$	$\chi_c/\%$
Nylon 6	176.2	221.5	80.0	15.0	65.0	27.0
N6C3.7	186.0	215.4	57.1	2.9	54.2	22.7

amplitude was fixed to 15% for nylon 6 and 10% for N6C3.7, respectively, to obtain reasonable signal intensities even at elevated temperature or low frequency ( $\omega$ ) to avoid the nonlinear response. For each sample investigated, the limits of linear viscoelasticity were determined by performing strain sweeps at a series of fixed  $\omega$ 's. The master curves were generated using the principle of time-temperature superposition and shifted to a common reference temperature ( $T_r$ ) of 225 °C, which was chosen as the most representative of a typical processing temperature of nylon 6.

### 3. Results and discussion

#### 3.1. Crystallization behavior

Fig. 1 shows the TMDSC thermograms of neat nylon 6 and N6C3.7 during cooling from melt state ( $\sim 260$  °C) and 2nd heating with a rate of 5 °C/min. For N6C3.7, the evolution of the crystallization peak is sharp and its maximum is at 186 °C. For the neat nylon 6, this peak is much broader and it appears at 176 °C. The dispersed MMT particles in N6C3.7 promote the crystallization possibly due to the nucleation effect. In the TMDSC experiments, the endothermic heat flow ( $\Delta H_{\text{difference}}$ ) of the initially existing crystallites can be easily calculated as  $\Delta H_{\text{difference}} = \Delta H_{\text{rev}} - \Delta H_{\text{nonrev}}$ , where  $\Delta H_{\text{rev}}$  is the endothermic melting (reversible) enthalpy from the reversing heat flow profile and  $\Delta H_{\text{nonrev}}$  is the exothermic ordering/crystallization (nonreversible) enthalpy from the nonreversing heat flow profile appearing in the temperature range of 150–230 °C. The estimate values of  $\chi_c$  are shown in Table 1. The presence of MMT particles cause a slight shift in the melting peak to slightly lower temperature (215.4 °C) and lower total crystallinity. In our previous observation [10], the lower  $T_m$  has been attributed to an increased fraction of  $\gamma$ -phase crystallites present in N6C3.7.

Figs. 2 and 3 represent the typical example of POM micrographs (with time variation at 190 °C) and the corresponding LS patterns (with a range of isothermal  $T_c$ ) under Hv optical alignment for neat nylon 6 and N6C3.7, respectively. The crystallization had been completed for 60 s. The clear spherulites with positive birefringence appeared and the four-leaf-clover patterns of Hv-LS pattern

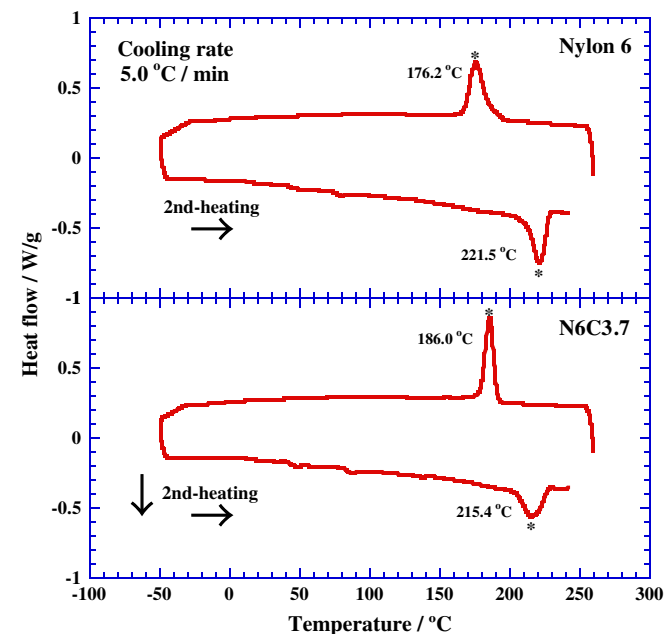


Fig. 1. TMDSC scans for neat nylon 6 and its nano-composite (N6C3.7).

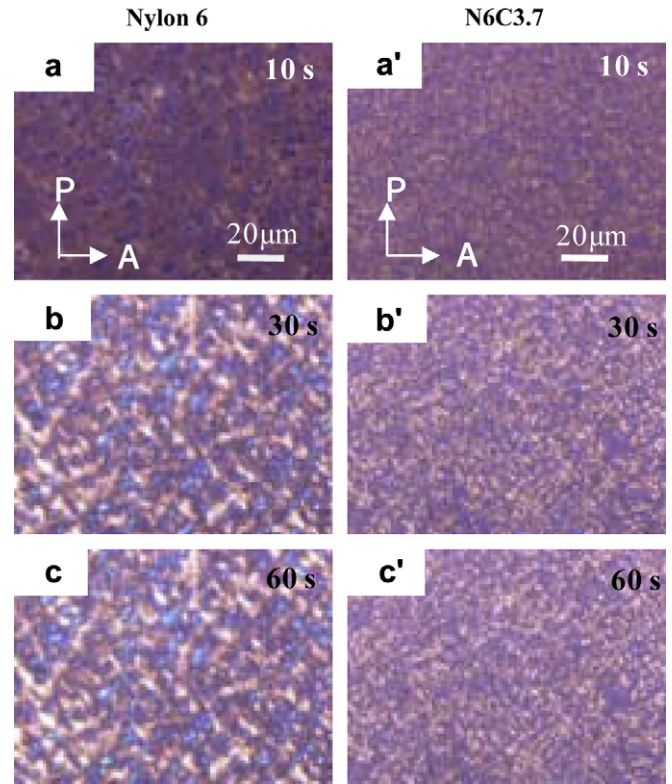


Fig. 2. Polarized optical micrographs with time variation for neat nylon 6 ((a)–(c)) and its nano-composite (N6C3.7) ((a')–(c')) isothermally crystallized at 190 °C.

were seen for the crystallized neat nylon 6. It is well known that at crystallization temperature (150–215 °C), neat nylon 6 crystallizes to form positive spherulites [26]. The clear four-leaf-clover patterns are due to the high ordering in both tangential and radial direction in the spherulite [26].

In contrast, for N6C3.7, the diffuse maltose cross patterns with very weak positive birefringence as seen in Fig. 2(a')–(c') and the rod-like pattern is observed clearly in Fig. 3(c')–(f) rather than four-leaf-clover pattern. The rod-like scattering pattern is ascribed to the parallel arrangement of radiation primary lamellae and the disordered arrangement of lamellae and the weak positive birefringence to the low density of the lamellae. The formation of the lamellae may be restricted due to small space ( $\cong \xi_{\text{MMT}}$ ) surrounded by the dispersed MMT particles in the nylon 6 matrix. These interesting features may be related with the formation of  $\gamma$ -phase crystallite of the crystallized N6C3.7.

#### 3.2. $\gamma$ -phase crystallite

The typical WAXD patterns of nylon 6 and N6C3.7 are shown in Fig. 4 to explain the formation of  $\gamma$ -phase crystallite. The assignment of the reflections associated with both  $\alpha$ - and  $\gamma$ -phases of nylon 6 are based on the unit cell and chain configurations reported in the literature [27]. In Fig. 4(a), the diffraction peaks at  $2\theta = 20.3^\circ$  and  $23.3^\circ$  correspond to the planes (200) and (002) + (202) of  $\alpha$ -phase crystallite (monoclinic unit cell), which will be hereafter defined as  $\alpha_1$  and  $\alpha_2$ , respectively. The diffraction peaks (020) and (011) planes of  $\gamma$ -phase crystallite (pseudo-hexagonal unit cell) appear at  $2\theta = 10.7^\circ$  and  $21.3^\circ$ , which will be hereafter defined as  $\gamma_1$  and  $\gamma_2$ , respectively. At lower  $T_c$  ( $=150$  °C), the neat nylon 6 exhibits both the extended all-trans  $\alpha$ -form and the pleated sheeted  $\gamma$ -form crystalline structure. With increasing  $T_c$ , the  $\gamma$ -form gradually decreases and vanishes at  $T_c = 215$  °C or higher

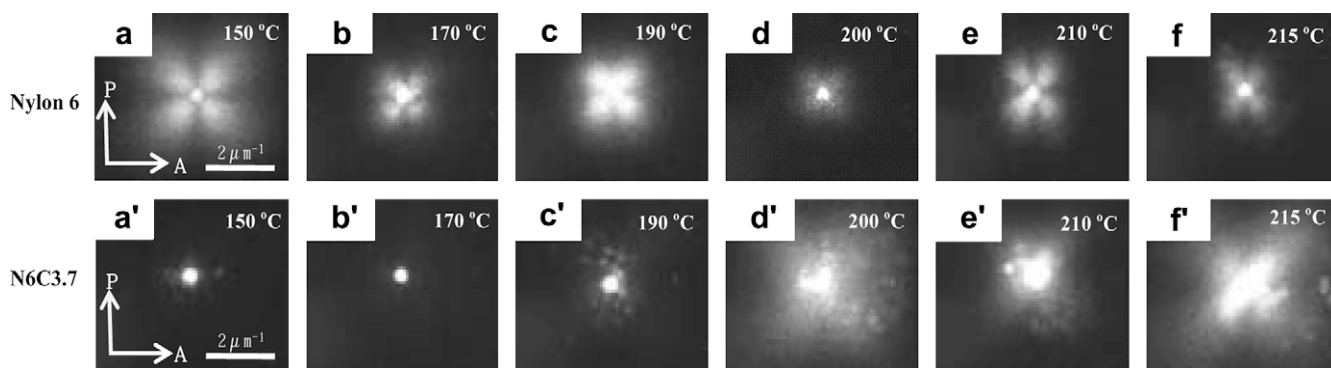


Fig. 3. Changes in light scattering patterns of neat nylon 6 ((a)–(f)) and N6C3.7 ((a')–(f')) at various  $T_c$  ranging from 150 to 215 °C.

temperature. On increasing  $T_c$ , the  $\alpha_2$  peak shifts to a higher angle, while the  $\alpha_1$  peaks remain constant angle. This suggests that the distance between chains bonded by van der Waals forces (i.e. hydrogen (H) bonded sheets) ( $\alpha_2$ ) decreases, whereas the distance between H-bonded chains ( $\alpha_1$ ) is constant up to  $T_c = 215$  °C. The Bragg  $d$ -spacing of  $\alpha_2$  is more sensitive to temperature compared with that of  $\alpha_1$ . That is, a variation of the interplanar distance is more rigid than in the direction of the van der Waals interactions [27]. During the rapid cooling due to the large supercooling ( $\equiv T_m^\circ - T_c$ ,  $T_m^\circ$  being equilibrium melting temperature), the formation of the most energetically stable  $\alpha$ -form could be hindered presumably due to lack of time for development.

On the contrary, N6C3.7 always exhibit mostly  $\gamma$ -form throughout the whole  $T_c$  range studied here. At higher  $T_c$  ( $=215$  °C), the  $\gamma_2$  peak shifts to a higher value, finally approaching  $2\theta = 21.5^\circ$ . The  $\gamma_1$  peak does not change and abruptly become a small remnant peak at  $T_c = 215$  °C. The longer  $d$ -spacing of the  $\gamma_1$  (020) crystal planes is most likely an effect of the strong hydrogen bonding interactions. The  $\gamma_2$  (011) planes are thermally stable compared with the (020) crystal planes.

### 3.3. Crystallization rate determined from light scattering

To understand the crystallization kinetics of neat nylon 6 and N6C3.7, we have used time-resolved LS photometry, which is a powerful tool for estimating the overall crystallization rate and its

kinetics in supercooled crystalline polymer liquid [28]. For the kinetics of crystallization, we can employ the integrated scattering intensity, i.e. the invariant  $Q$  is defined as

$$Q = \int_0^\infty I(q)q^2 dq \quad (1)$$

where  $q$  (scattering vector  $= (4\pi/\lambda_{LS}) \sin(\theta_{LS}/2)$ ) and  $I(q)$  is the intensity of the scattered light at  $q$  [28].

In the  $H_V$  mode the invariant  $Q_\delta$  can be described by the mean-square optical anisotropy  $\langle \delta^2 \rangle$ :

$$Q_\delta \propto \langle \delta^2 \rangle \propto \phi_s (\alpha_r - \alpha_t)^2 \quad (2)$$

where  $\phi_s$  is the volume fraction of spherulites, and  $\alpha_r$  and  $\alpha_t$  are the radial and tangential polarizabilities of spherulites, respectively. We constructed a plot of reduced invariant  $Q_\delta/Q_\delta^\infty$  versus time  $t$  with  $Q_\delta^\infty$  being  $Q_\delta$  at an infinitely long time of crystallization (up to full solidification of the melt).

Fig. 5 shows the time variation of the invariant  $Q_\delta/Q_\delta^\infty$  taken for neat nylon 6 and N6C3.7 at same supercooling ( $\Delta T$ ) ( $=T_m^\circ - T_c$ ) ( $\cong 11$  °C). From the onset time  $t_0$  we can estimate the induction time of the crystallization until start of crystallization, and we plotted it in Fig. 6 against  $\Delta T$ . The value of  $T_m^\circ$  can be determined by Hoffman–Weeks [29] extrapolation based on plotting  $T_m$  against  $T_c$  (see Fig. 7). As seen in Fig. 7, we see quite a different behavior in

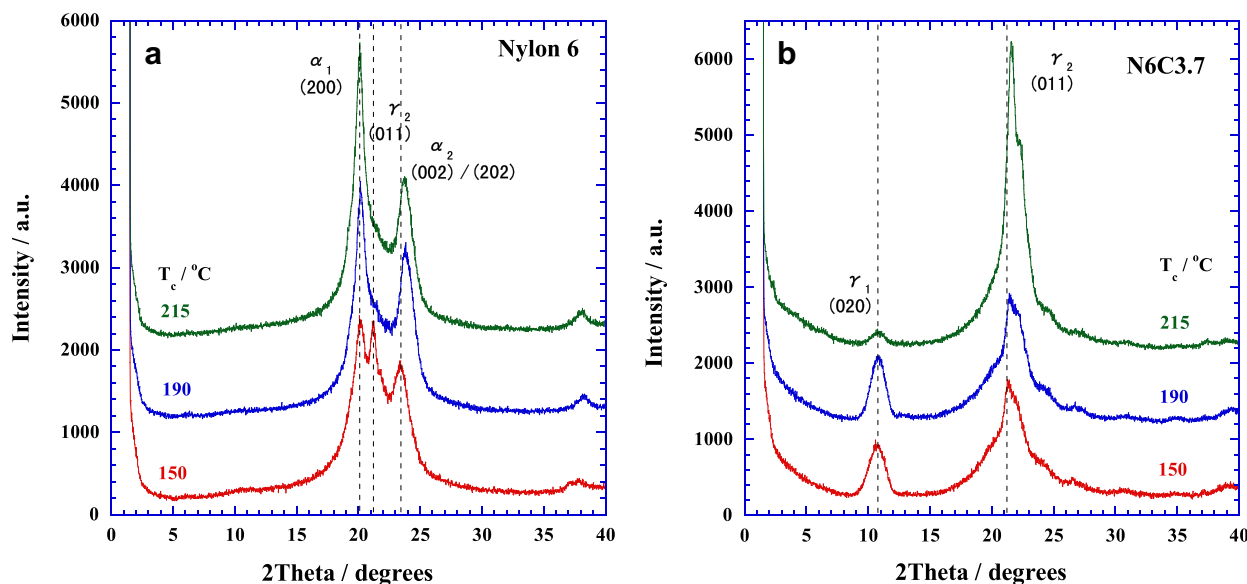


Fig. 4. Typical WAXD profiles of (a) neat nylon 6 and (b) N6C3.7 crystallized at 150, 190 and 215 °C. The curves are vertically offset for clarity.

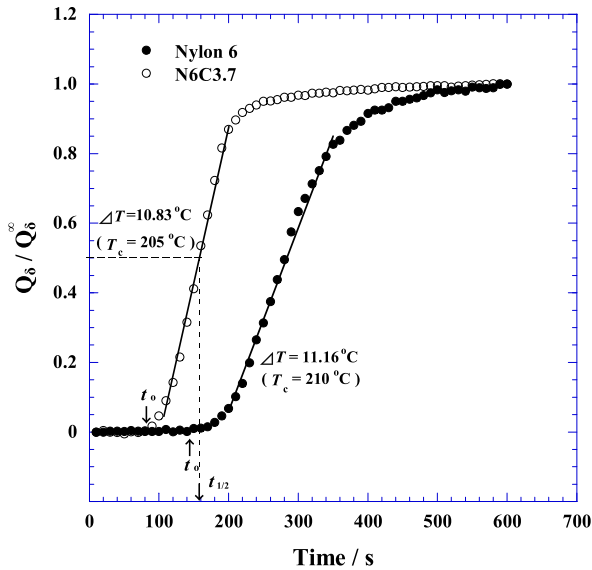


Fig. 5. Time variation of reduced invariant  $Q_{\delta}/Q_{\delta}^{\infty}$  during isothermal crystallization at same supercooling ( $\Delta T$ ) ( $\cong 11$  °C). The solid line represents the slope (overall crystallization rate). The arrows indicate the induction time of crystallization. The dashed line indicates the crystallization half-time  $t_{1/2}$ .

N6C3.7 between 150–200 °C range and the 210–220 °C range. In the 150–200 °C annealing (isothermal crystallization), the estimated value of  $T_m^{\circ}$  by extrapolation is 215.8 °C. Above 200 °C annealing the higher values of  $T_m^{\circ}$  seem to be the increase of the average lamellar thickness.  $T_m^{\circ}$  decreases by 5.4 °C for N6C3.7 ( $T_m^{\circ} = 215.8$  °C) as compared to the neat nylon 6 ( $T_m^{\circ} = 221.2$  °C), although there is controversy surrounding the determination of  $T_m^{\circ}$  obtained from two different crystal forms as discussed in Fig. 4. The value of  $\Delta H_{\text{difference}}$  also decreases in the nano-composite (N6C3.7) in comparison to that of the neat nylon 6, which strongly suggests a greater interacting nature of the nylon 6 matrix and MMT particles.

In Fig. 6, at all  $T_c$  measured here the  $t_0$  value for N6C3.7 is lower than that of neat nylon 6. In the changes in  $t_0$  with  $\Delta T$ , the N6C3.7

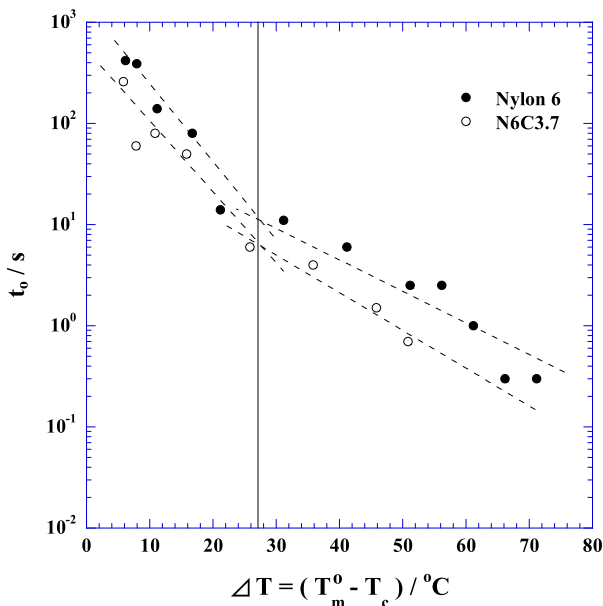


Fig. 6.  $\Delta T$  dependence of induction time for neat nylon 6 and N6C3.7.

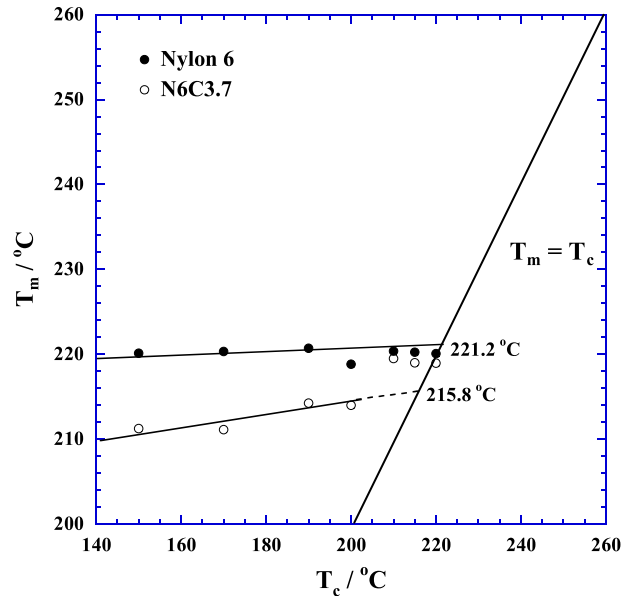


Fig. 7. Hoffman–Weeks plots for neat nylon 6 and N6C3.7 crystallized isothermally at various temperatures.

shows short time especially at large  $\Delta T$ , suggesting that the dispersed MMT particles have some contribution to enhance the nucleation.

As seen in Table 1, the higher  $T_{cc}$  value for N6C3.7 ( $T_{cc} = 186.0$  °C) suggests that the nano-composite is more easily crystallizable as compared with neat nylon 6 ( $T_{cc} = 176.2$  °C) during the TMDSC cooling process.

The overall crystallization rate was determined from the slope  $Q_{\delta}/Q_{\delta}^{\infty}$  ( $d(Q_{\delta}/Q_{\delta}^{\infty})/dt$ ) in the crystallization region as indicated by the solid line in Fig. 5. It is clear that the overall crystallization rate increases in N6C3.7, in comparison to the neat nylon 6. The same trend is also observed over the wide range of  $\Delta T$  studied here.

In order to compare the crystallization rate, we assume heterogeneous nucleation and apply the Hoffman–Lauritzen growth rate equation slow kinetics [30,31] even if we are not using the analysis to determine linear growth rates. The growth rate of crystal can be written as

$$\text{Overall rate} \propto \beta_g \exp \left[ -\frac{K_g}{T_c(\Delta T)f} \right] \quad (3)$$

where  $\beta_g$  is a mobility term, which describes the transportation rate of crystallizable molecules to the growth front;  $f$  is the correction factor given by  $2T_c/(T_m^{\circ} + T_c)$ ; and  $K_g$  is the nucleation constant, which depends on the crystallization regime (regime I, single nucleation; regimes II and III, multiple nucleation) [30,32]. At small supercoolings and over limited temperature range, the temperature dependence of growth is determined predominantly by the nucleation term. Accordingly, assuming that the  $(d(Q_{\delta}/Q_{\delta}^{\infty})/dt)$  is a satisfactory measure to the rate of crystallization, we plot the data as  $(d(Q_{\delta}/Q_{\delta}^{\infty})/dt)$  versus  $1/(T_c\Delta T f)$ : see Fig. 8.

The overall rate of N6C3.7 is enhanced for every temperature of measurement. For both systems, a change in slope at  $1/(T_c\Delta T f) \cong 1.30 \times 10^{-4} \text{ K}^{-2}$  corresponding to  $\Delta T \cong 16\text{--}17$  °C is obvious. At higher  $T_c$  range ( $\Delta T < 27$  °C), a retarding effect of the crystal growth is observed. This feature is superficially similar to the result as shown in Fig. 6. A similar change on supercooling is found at  $\Delta T \cong 27$  °C. Therefore it can be assumed that a disturbed crystal growth occurs as the supercooling decreases and the system crystallized by regime I mechanism [32].

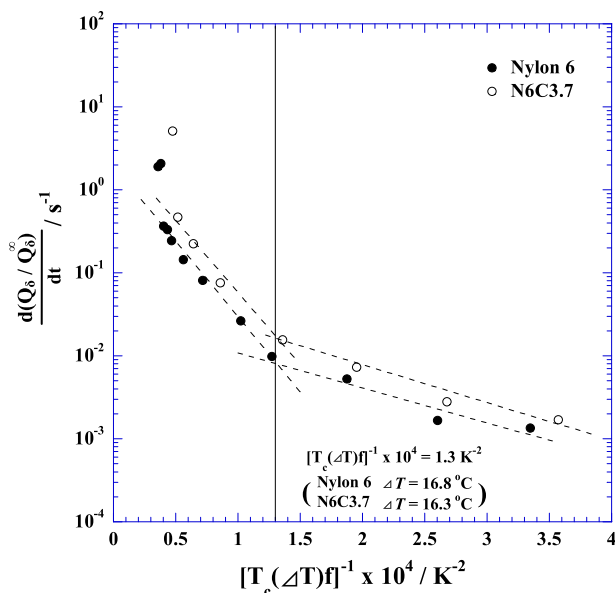


Fig. 8. The plot of overall crystallization rate versus  $1/(T_c\Delta T)$  for different  $T_c$  in neat nylon 6 and N6C3.7. The solid line indicates  $1/(T_c\Delta T) = 1.3 \times 10^{-4} \text{ K}^{-2}$  ( $\Delta T = 16.8^\circ\text{C}$  for nylon 6 and  $\Delta T = 16.3^\circ\text{C}$  for N6C3.7, respectively).

### 3.4. Melt rheology and relaxation time

The rheological properties of in-situ polymerized nano-composites with end-tethered polymer chains were first described by Krishnamoorti and Giannelis [33]. The flow behavior of nylon 6-based nano-composites differed extremely from that of the corresponding neat matrix, whereas the thermorheological properties of the nano-composites were entirely determined by that behavior of matrix [33]. The slope of  $G'(\omega)$  and  $G''(\omega)$  versus the  $a_T\omega$  is much smaller than 2 and 1, respectively. Values of 2 and 1 are expected for linear mono-dispersed polymer melts, and are large deviation especially in the presence of very small amount of layered silicate loading may be due to the formation of network structure in the melt state [34].

As seen in Fig. 9, in the linear viscoelastic regime, a big change in terminal (low frequency  $a_T\omega < 1 \text{ rad s}^{-1}$ ) region from liquid-like response to a solid-like response was observed for N6C3.7 ( $G'(\omega) \sim G''(\omega) \propto \omega^{0.4}$ ), ascribed to the formation of a volume spanning mesoscale MMT network above the mechanical percolation threshold [35]. The terminal rheology is sensitive to MMT loading and extent of exfoliation in the polymer matrix [33,34].

This mesoscale structure is partially supported by transmission electron microscopic (TEM) observation [10] (see Fig. 13 in Appendix). The correlation length between MMT particles  $\xi_{\text{MMT}}$  ( $\cong 20 \text{ nm}$ ) is smaller than average value of the particle length  $L_{\text{MMT}}$  ( $\cong 100 \text{ nm}$ ) for N6C3.7, suggesting the formation of the highly geometric constraints. A plausible explanation and its model are presented by Ren et al. [36]. The individual or stacked silicate layers are incapable of freely rotating and hence, by imposing small  $\omega$ , the relaxation of the structure are prevented almost completely. This type of prevented relaxation leads to the presence of the volume spanning mesoscale network. The effective volume occupied by the clay platelets is much larger than may be calculated from their volume alone. At the same time, the pseudo-solid like behavior is generated in N6C3.7.

The temperature dependence frequency shift factor ( $a_T$ , Arrhenius-type) used to generate master curves shown in Fig. 9 are shown in Fig. 10. The dependence of the frequency shift factors on the MMT loading suggests that the temperature-dependent

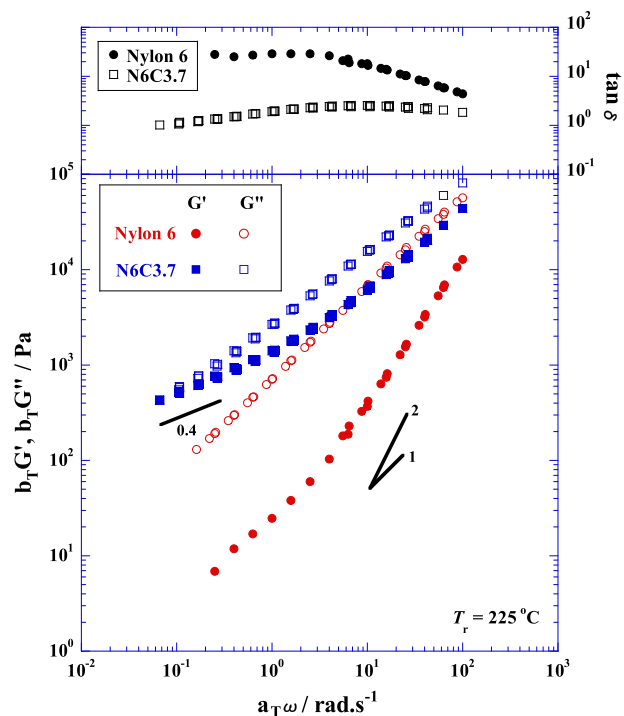


Fig. 9. Reduced frequency dependence of storage modulus  $G'(\omega)$ , loss modulus  $G''(\omega)$  and  $\tan \delta$  of neat nylon 6 and N6C3.7 at  $T_r = 225^\circ\text{C}$ . The solid line was drawn by the power law of  $G'(\omega) \sim G''(\omega) \sim \omega^{0.4}$  in the low  $\omega$  region.

relaxation process observed in the viscoelastic measurements are affected by the presence of the silicate layers. In the case of N6C3.7, where the hydrogen-bonding on the already formed hydrogen-bonded molecule to the silicate surface [10], the system exhibits large value of flow activation energy near one order higher in magnitude compared with that of the neat nylon 6 (see Table 2).

The shift factor  $b_T$  shows large deviation from a simple density effect, it would be expected that the values would not vary far from unity ( $b_T = \rho T / \rho_f T_f$ , where  $\rho$  and  $\rho_f$  are the density at  $T$  and  $T_f$ , respectively) [37]. One possible explanation is a network structural

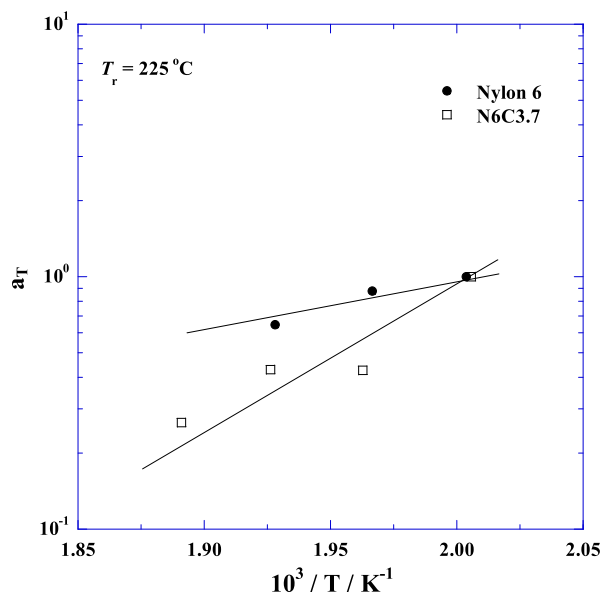


Fig. 10. Frequency shift factors  $a_T$  as a function of temperature ( $T_r = 225^\circ\text{C}$ ).

**Table 2**  
Vertical shift factor ( $b_T$ ) and flow activation energy ( $E_a$ ) for ionomers and nanocomposites.

Samples	$T/^\circ\text{C}$	$b_T$	$E_a^a/\text{kJ/mol}$
Nylon 6	225 (=T <sub>r</sub> )	1.00	37.9
	235	1.0	
	245	1.0	
N6C3.7	225 (=T <sub>r</sub> )	1.0	111.2
	235	0.9	
	245	1.7	
	255	2.2	

<sup>a</sup> We investigated the low frequency values of complex viscosity ( $|\eta^*|$ ) as a function of temperature in each system. At temperature where a zero-shear value was not obtained experimentally, a combination of time-temperature superposition and fitting using the Ellis model was employed to obtain a zero-shear viscosity ( $|\eta^*|$ ) from a master curve. The values are calculated from Arrhenius-type equation given as  $|\eta^*| \sim \exp(E_a/RT)$ .

change occurring in N6C3.7 during measurement (shear process). The reconstituting of the layered silicate network probably supports for the melt under weak shear flow (terminal zone), thereby leads to the increase in the absolute values of  $G'(\omega)$  and  $G''(\omega)$ .

To understand the generic dynamic rheology, the cross over frequency  $\omega_{\text{rel}}$  in the master curve of the dynamic frequency sweep enables one to predict a relaxation time ( $=1/\omega_{\text{rel}}$ ), which is determined from the measured master curve when  $\tan \delta$  is unity. Fig. 11 shows the results of the temperature dependence of relaxation rate ( $\omega_{\text{rel}}$ ), assuming that the rate is of Arrhenius-type. In order to discuss the correlation between the chain mobility of the nylon 6 and the growth mechanism of the  $\gamma$ -form crystals, we define  $1/t_{1/2}$  as a measure of the crystallization rate, taking the crystallization half-time ( $t_{1/2}$ ) at which the reduced intensity reaches 1/2 in Fig. 5, and we plotted it in Fig. 11 against  $1/T$ . Furthermore, in Fig. 11, we present the temperature dependence of the rotational relaxation rate ( $1/t_d$ ), which is given by

$$1/t_d \sim \left[ \frac{(\pi/2)^2}{D_{r0}} \right]^{-1} \quad (4)$$

A quarter period is provided to complete rotational relaxation. In the equation (4), the rotary diffusivity ( $D_{r0}$ ) of a circular disk (MMT

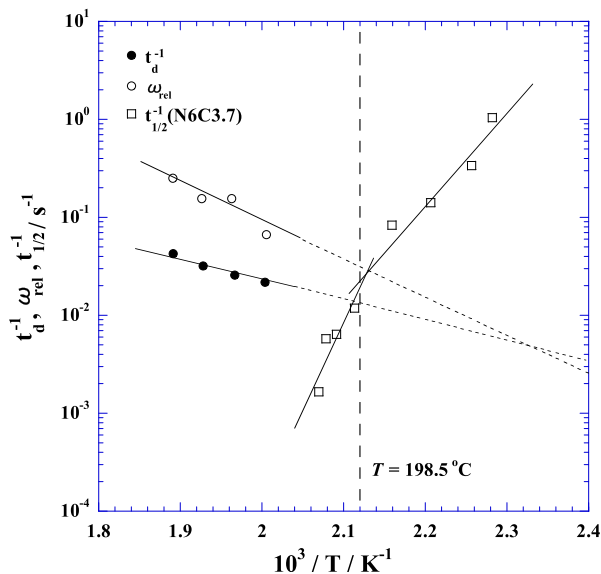


**Fig. 11.** Temperature dependence of characteristic relaxation rates ( $\omega_{\text{rel}}$  and  $1/t_d$ ) and crystallization rate ( $1/t_{1/2}$ ) of N6C3.7.

particle) of radius ( $d$ ) ( $=L_{\text{MMT}}/2$  ( $=50$  nm)) is simply argued by Brownian motion [38,39]. The rotary diffusivity is given by

$$D_{r0} = \frac{3k_B T}{4\eta_0 d^3} \quad (5)$$

where  $\eta_0$  is the neat nylon 6 matrix viscosity ( $\cong \eta_0^*$ ) at any temperatures,  $k_B$  is the Boltzmann constant, and  $T$  is the temperature. This time scale ( $t_d$ ) is useful to discuss the reconstituting of the network via the rotation of the MMT particles as compared with experimental time scale.

For N6C3.7, the estimated time scale for rotational relaxation rates is about  $0.02$ – $0.04$  s<sup>-1</sup> in the range of temperature between  $225$  and  $255$  °C. These values are much smaller than the relaxation time scale ( $1/\omega_{\text{rel}}$ ) (those are in fact  $0.066$ – $0.25$  s<sup>-1</sup>), suggesting the major driving force for the structural evolution (relaxation of the mesoscale network) is not simple Brownian relaxation of the MMT particles. The slope that reflects the activation energy of each process exhibits different value. The activation energy of the crystallization process is also estimated in the two range of temperature blow and above  $T \cong 199$  °C. The calculated values are presented in Table 3. Interestingly, the activation energy of the crystallization process exhibits large value one order higher in magnitude compared with those of the relaxation of the network and particle rotation. Another interesting feature is that in the range of temperature between  $200$  and  $210$  °C we could attain a high enough relaxation rate of the network by extrapolation based on plotting  $\omega_{\text{rel}}$  versus  $1/T$  as compared with the crystallization rates, so that the retarding effect might be overwhelmed.

On the other hand, at  $T_c = 160$ – $190$  °C the crystallization with large  $\Delta T$  provides the disturbed crystal growth and hinder the stable growth of the  $\gamma$ -form due to the lack of time for crystalline structure development. This is supported by the TEM observation.

### 3.5. $\gamma$ -form morphology

The lamellar morphology and distribution of MMT particles in N6C3.7, crystallized at  $170$  and  $215$  °C, have been shown in Fig. 12. The white strips represent the discrete lamellar pattern, and after a close look, shown in the enlarged view, we clearly observe a black MMT particle inside the lamella. In other words, the lamellar growth occurs on both sides of the dispersed MMT particles, i.e. the MMT particle is sandwiched by the lamella formed. The thickness of the developed lamella is around  $5$  nm. This is a unique observation of the lamellar orientation on the silicate layers. In the semi-crystalline polymer generally we observe the stacked lamellar orientation [40]. The lamellar pattern at high  $T_c$  ( $=215$  °C) (Fig. 12(b)) is somehow similar but along with the sandwiched structure, branched lamellae are formed which were originated from the parent sandwiched lamella. There are no silicate particles inside the branch lamella and the  $\gamma$ -phase is formed as revealed by WAXD (see Fig. 4(b)). The thickness of the branch lamella is around  $4$  nm. This value is smaller than that of the parent sandwiched lamella. The difference just corresponds to the thickness of the individual silicate layer ( $\sim 1$  nm). This epitaxial growth ( $\gamma$ -phase) on the parent lamella forms the *shish-kebab* type of structure,

**Table 3**  
Activation energy of each process in N6C3.7.

Process	$T$ -range/ $^\circ\text{C}$	$E_a/\text{kJ/mol}$
$\omega_{\text{rel}}$	225–255	87.9
$1/t_d$	225–255	48.3
$1/t_{1/2}$	160–190	195.9
$1/t_{1/2}$	200–210	318.3

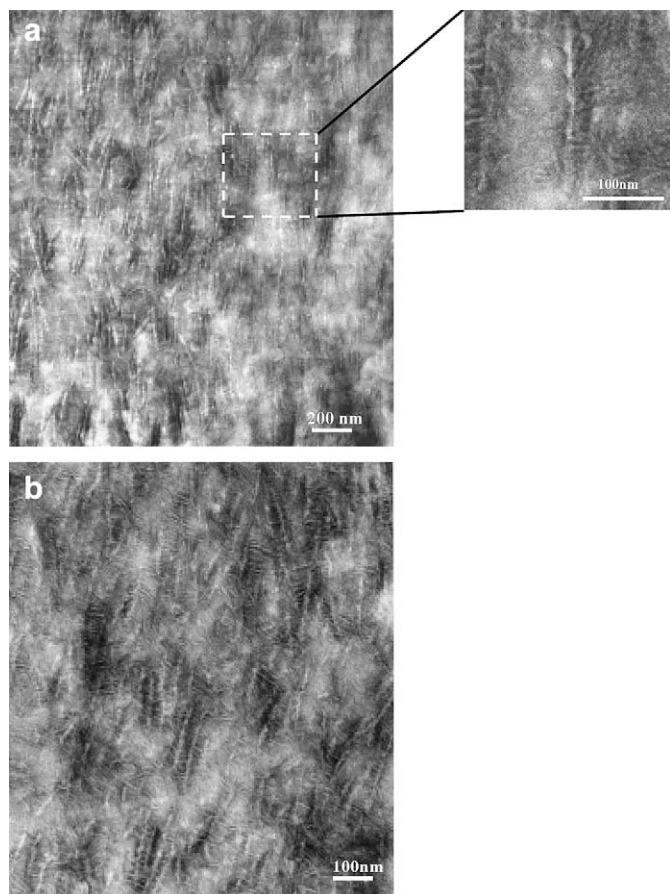


**Fig. 12.** Bright field TEM images of N6C3.7 crystallized at (a) 170 °C and (b) 215 °C. The enlarged part shown (Fig. 12(a)) forms the indicated lamellae in the original image. The black strip inside the white part is an individual MMT particle. Fig. 12(b) shows the typical *shish-kebab* type of structure.

which virtually enhances the mechanical properties of the nano-composites [6–8]. As a consequence, at low  $T_c$  (=150–190 °C), the reduction of the chain mobility of the nylon 6 might lead to smaller, less-ordered  $\gamma$ -form crystallites. For this reason, we could not observe clear LS patterns under Hv optical alignment (see Fig. 3). All

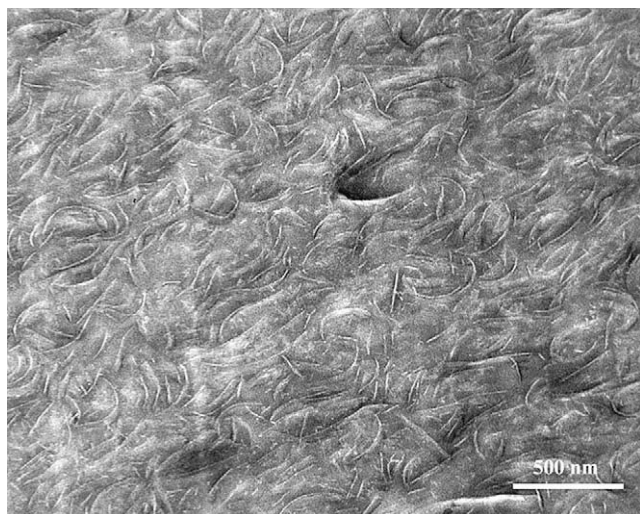


**Fig. 13.** Bright field TEM images of N6C3.7 crystallized during slow cooling process as shown in TMDSC scan (Fig. 1).

these behaviors appear to arise from the exclusive formation of the  $\gamma$ -phase in the presence of MMT particles.

#### 4. Conclusions

The detailed crystallization kinetics and crystalline morphology of neat nylon 6 and nano-composite (N6C3.7) have been investigated. The neat nylon 6 predominantly formed  $\alpha$ -phase in the crystallization temperature range of 150–215 °C coexisting with the small evolution of pseudo-hexagonal  $\gamma$ -form crystals at low  $T_c$  range (150–190 °C). On the other hand, N6C3.7 exhibited  $\gamma$ -phase crystal due to the nucleating effect of the dispersed MMT particles into the nylon 6 matrix throughout the whole  $T_c$  range (=150–215 °C) as revealed by WAXD, DSC and LS analyses. The lamellar growth of the  $\gamma$ -phase crystal took place on both sides of the dispersed MMT particles. The overall crystallization rate on nylon 6 increased after nano-composite formation as compared with that of the neat nylon 6.

The formation of the network structure owing to the dispersed MMT particles affected the lamellar growth of the  $\gamma$ -phase crystal. At low  $T_c$  (=150–190 °C), the crystal growth of the  $\gamma$ -form was disturbed due to the lack of time for crystallization as revealed by the relaxation time analysis. For this reason, the stable growth of the branch lamellae occurred at high  $T_c$  (=215 °C) accompanied with the *shish-kebab* type of structure formation.

#### Acknowledgments

This work was supported by the MEXT “Collaboration with Local Communities” Project (2005–2009).

#### Appendix. Nano-composite structure

Fig. 13 shows the results of TEM bright field images of N6C3.7, in which white entities are the cross section of the discrete lamella and the dark area is the nylon 6 matrix due to the staining with 12 tungstophosphoric acid at 80 °C for 2 h. The black strip inside the white part is an individual (exfoliated) MMT particle. The silicate layers are more homogeneously and finely dispersed. The figure shows larger view permitting the observation of discrete nanolayers. The disorder and delaminated layer structure are observed in the TEM image. We estimated the form factors obtained from TEM images, i.e. average value of the particle length ( $L$ ), thickness ( $D$ ), of the dispersed particles and the correlation length ( $\xi$ ) between the particles. The details of the evaluation were described in our previous paper [41]. For N6C3.7,  $L$ ,  $D$  and  $\xi$  are in the range of 1–2 nm,  $100 \pm 10$  nm and are  $20 \pm 5$  nm, respectively. The  $\xi$  value ( $\cong 20$  nm) corresponds to the random coil size of nylon 6 in N6C3.7. The root-mean-square radius of gyration  $\langle S^2 \rangle^{1/2}$  is around 9 nm, which is calculated by  $\langle S^2 \rangle^{1/2} = 4.0 \times 10^{-2} M_w^{1/2}$  [42]. The chain mobility of the nylon 6 presumably is decreased in translational motion.

#### References

- [1] Sinha Ray S, Okamoto M. Prog Polym Sci 2003;28:1539.
- [2] Vaia RA, Wagner HD. Mater Today 2004;7:32.
- [3] Gao F. Mater Today 2004;7:50.
- [4] Okamoto M. Mater Sci Technol 2006;22:756.
- [5] Okada A, Usuki A. Macromol Mater Eng 2006;291:1449.
- [6] Usuki A, Kawasumi M, Kojima Y, Okada A, Kurauchi T, Kamigaito O. J Mater Res 1993;8:1179.
- [7] Kojima Y, Usuki A, Kawasumi M, Okada A, Fukushima Y, Kurauchi T, et al. J Mater Res 1993;8:1185.
- [8] Usuki A, Koiwai A, Kojima Y, Kawasumi M, Okada A, Kurauchi T, et al. J Appl Polym Sci 1995;55:119.
- [9] Lincoln DM, Vaia RA, Wang ZG, Hsiao BS. Polymer 2001;42:1621.
- [10] Maiti P, Okamoto M. Macromol Mater Eng 2003;288:440.

- [11] Holes DR, Bunn CW, Smith DJ. *J Polym Sci* 1955;17:159.
- [12] Mathias L, Davis R, Jarrett W. *Macromolecules* 1999;32:7958.
- [13] Kojima Y, Usuki A, Kawasumi M, Okada A, Kurauchi T, Kamigaito O, et al. *J Polym Sci Part B Polym Phys* 1994;32:625.
- [14] Lincoln DM, Vaia RA, Wang ZG, Hsiao BS, Krishnamoorti R. *Polymer* 2001;42:9975.
- [15] Medellin-Rodriguez FJ, Burger C, Hsiao BS, Chu B, Vaia RA, Phillip S. *Polymer* 2001;42:9015.
- [16] Kamal MR, Borse NK, Garcia-Rejion A. *Polym Eng Sci* 2002;42:1883.
- [17] Nair SS, Ramesh C. *Macromolecules* 2005;38:454.
- [18] Bertmer M, Wang M, Kruger M, Blumich B, Litvinov VM, van Es M. *Chem Mater* 2007;19:1089.
- [19] Fornes TD, Paul DR. *Polymer* 2003;44:3945.
- [20] Homminga DS, Goderis B, Mathot VBF, Groeninckx G. *Polymer* 2006;47:1630.
- [21] Miltner HE, Van Assche G, Pozsgay A, Pukanszky B, Van Mele B. *Polymer* 2006;47:826.
- [22] Wang K, Liang S, Deng J, Yang H, Zhang Q, Fu Q, et al. *Polymer* 2006;47:7131.
- [23] Nam PH, Maiti P, Okamoto M, Kotaka T, Hasegawa N, Usuki A. *Polymer* 2001;42:9633.
- [24] Illers KH. *Makromol Chem* 1978;179:497.
- [25] Kubo H, Sato H, Okamoto M, Kotaka T. *Polymer* 1998;39:501.
- [26] Khoury F. *J Polym Sci* 1958;33:389.
- [27] Arimoto H, Ishibashi M, Hirai M, Chatani Y. *J Polym Sci Part A Polym Chem* 1965;3:317.
- [28] Okamoto M, Inoue T. *Polymer* 1995;36:2736.
- [29] Martuscelli E, Silvestre S, Abate G. *Polymer* 1982;23:229.
- [30] Lauritzen JJ, Hoffman JD. *J Appl Phys* 1973;44:4340.
- [31] Hoffman JD, Froln LJ, Ross GS, Lauritzen JJ. *J Res Natl Bur Stand (A)* 1975;79:671.
- [32] Hoffman JD. *Polymer* 1983;24:3.
- [33] Krishnamoorti R, Giannelis EP. *Macromolecules* 1997;30:4097.
- [34] Sinha Ray S, Yamada K, Okamoto M, Ueda K. *Polymer* 2003;44:6631.
- [35] Treece MA, Oberhauser JP. *Polymer* 2007;48:1083.
- [36] Ren J, Silva AS, Krishnamoorti R. *Macromolecules* 2000;33:3739.
- [37] Williams ML, Landel RF, Ferry JD. *J Am Chem Soc* 1955;77:3701.
- [38] Brenner H. *Int J Multiphase Flow* 1974;1:195.
- [39] Ren J, Casanueva BF, Mitchell CA, Krishnamoorti R. *Macromolecules* 2003;36:4188.
- [40] Kim GM, Lee DH, Hoffmann B, Kressler J, Stoppelmann G. *Polymer* 2001;42:1095.
- [41] Sinha Ray S, Yamada K, Okamoto M, Ogami A, Ueda K. *Chem Mater* 2003;15:1456.
- [42] Anastasiadis SH, Russel TP, Satija SK, Majkrzak CF. *J Chem Phys* 1990; 92:5677.